Pattern formation in a model of competing populations with nonlocal interactions

B.L. Segal [1], V.A. Volpert, A. Bayliss *

Department of Engineering Sciences and Applied Mathematics, Northwestern University, Evanston, IL 60208-3125, USA

HIGHLIGHTS

- Found nonlinear island/deadzone patterns for populations with nonlocal coupling.
- Characterize patterns using only model parameters and the pattern period.
- Demonstrated high degree of multiplicity of patterns.

ARTICLE INFO

ABSTRACT

We analyze and compute an extension of a previously developed population model based on the well-known diffusive logistic equation with nonlocal interaction, to a system involving competing species. Our model involves a system of nonlinear integro-differential equations, with the nonlocal interaction characterized by convolution integrals of the population densities against specified kernel functions. The extent of the nonlocal coupling is characterized by a parameter δ so that when $\delta \rightarrow 0$ the problem becomes local. We consider critical points of the model, i.e., spatially homogeneous equilibrium solutions. There is generally one critical point in the first quadrant (i.e., both population densities positive), denoting coexistence of the two species. We show that this solution can be destabilized by the nonlocal coupling and obtain general conditions for stability of this critical point as a function of δ, the specific kernel function and parameters of the model. We study the nonlinear behavior of the model and show that the populations can evolve to localized cells, or islands. We find that the stability transition is supercritical. Near the stability boundary solutions are small amplitude, nearly sinusoidal oscillations, however, when δ increases large amplitude, nonlinear states are found. We find a multiplicity of stable, steady state patterns. We further show that with a stepfunction kernel function the structure of these islands, a highly nonlinear phenomenon, can be described analytically. Finally, we analyze the role of the kernel function and show that for some choices of kernel function the resulting population islands can exhibit tip-splitting behavior and island amplitude modulation.

© 2013 Elsevier B.V. All rights reserved.

1. Introduction

In this paper we analyze a model of competing species with nonlocal interactions. The model developed in [1] is based on the well-known diffusive logistic model (Fisher equation) and extends the scalar model to account for two competing species. The nonlocal coupling is via convolution integrals with specified kernel functions.

The scalar model, together with an extension that incorporated nonlocality in time, was studied in [1,2]. The model admits a single spatially homogeneous and stationary equilibrium. Conditions for instability of this equilibrium, in terms of parameters of the problem, were determined. A discrete model related to the continuous model was studied in [3] and conditions for instability obtained.

Additional studies of the spatially nonlocal scalar problem were described in [4,5] and for a slightly modified scalar problem in [6]. Conditions for instability of homogeneous equilibria were obtained in terms of properties of the convolution kernel function. It was shown that instability required that the Fourier transform of the kernel function be negative for some band of wavenumbers. Several different nonlocal kernel functions were considered and stability boundaries were determined as functions of the parameters of the kernel function.

A linear stability analysis for the scalar problem, analogous to the analysis carried out below for the system, was performed in [7] for the case when the convolution kernel function was a stepfunction. The emergence of stationary patterns was then studied via

* Corresponding author. Tel.: +1 847 491 3345; fax: +1 847 491 2178.
E-mail address: a-bayliss@northwestern.edu (A. Bayliss).
[1] Present address: Department of Applied Mathematics, University of Washington, Seattle, WA 98195-2420, USA.

numerical simulations and it was shown that in the instability region, small perturbations evolved to nonlinear stationary states involving islands of nonzero population, separated by apparent deadzones where the population was essentially extinct. Propagating wave solutions were also found for asymmetric kernel functions.

In this paper we consider a model of two competing populations with nonlocal coupling. The extent of the coupling is described by a parameter δ so that when $\delta \to 0$ the coupling becomes local and the population satisfies a system of Fisher type partial differential equations for two competing species. We determine critical points, i.e., spatially homogeneous equilibrium solutions to the local problem. The critical point of most interest is one permitting coexistence of the two species. We consider the case where this equilibrium is stable for the problem with local coupling, but is destabilized by the nonlocal coupling i.e., for δ sufficiently large. We find that this transition is supercritical, as δ increases past the transition value, small amplitude, nearly sinusoidal oscillations occur. As δ increases further, we then find, using numerical computations, nonlinear states consisting of arrays of islands (regions of nonzero population) and deadzones (regions where the populations are essentially extinct). We also show how the structure of the islands can be described analytically when the kernel function is a stepfunction.

We next describe the model in detail. The model, introduced in [1], consists of two coupled integro-differential equations,

$$u_t = d_1 u_{xx} + k_1 u \left(1 - a_1 \phi_\delta * u - b_1 \phi_\delta * v\right) - p_1 u, \tag{1a}$$
$$v_t = d_2 v_{xx} + k_2 v \left(1 - a_2 \phi_\delta * u - b_2 \phi_\delta * v\right) - p_2 v. \tag{1b}$$

Here u and v are the population densities for the two competing species, t and x denote time and space, respectively, u_t and u_{xx} denote partial derivatives and $*$ denotes spatial convolution, i.e.,

$$\phi_\delta * w(x) = \int_{-\infty}^{\infty} \phi_\delta(x - y) w(y) dy, \tag{2}$$

where ϕ_δ is a specified function such that

$$\int_{-\infty}^{\infty} \phi_\delta(y) \, dy = 1. \tag{3}$$

We also assume that ϕ_δ is an even, nonnegative function with support in the interval $-\delta \le y \le \delta$. These conditions on ϕ_δ imply that ϕ_δ approaches a δ-function as $\delta \to 0$, thus the coupling is local in this limit.

For each of the two species (u and v), the first term on the right hand side of (1) describes diffusion, with diffusivities d_1 and d_2, respectively. The remainder of the right hand side describes the net reproductive rate of the species (birth rate minus the death rate). The terms

$$k_1 u - p_1 u = c_1 u, \qquad k_2 v - p_2 v = c_2 v, \tag{4}$$

describe the natural net birth rate for the two species. As is typical for population models based on the logistic equation we always assume that $c_i = k_i - p_i > 0$, $i = 1, 2$, so that the extinction solution ($u = v = 0$) is unstable. The quadratic terms

$$-k_1 a_1 u \phi_\delta * u = -\tilde{a}_1 u \phi_\delta * u, \tag{5a}$$
$$-k_2 b_2 v \phi_\delta * v = -\tilde{b}_2 v \phi_\delta * v, \tag{5b}$$
$$-k_1 b_1 u \phi_\delta * v = -\tilde{b}_1 u \phi_\delta * v, \tag{5c}$$
$$-k_2 a_2 v \phi_\delta * u = -\tilde{a}_2 v \phi_\delta * u, \tag{5d}$$

describe the decreased birth rate (or enhanced death rate) due to intraspecies ((5a), (5b)) and interspecies ((5c) and (5d)) competition, respectively. In the limit $\delta \to 0$ these terms reduce to the

standard quadratic terms of the logistic equation. Using the terminology in (4) and (5) the system (1) can be written in the simpler form

$$u_t = d_1 u_{xx} + c_1 u - u \left(\tilde{a}_1 \phi_\delta * u + \tilde{b}_1 \phi_\delta * v\right), \tag{6a}$$

$$v_t = d_2 v_{xx} + c_2 v - v \left(\tilde{a}_2 \phi_\delta * u + \tilde{b}_2 \phi_\delta * v\right). \tag{6b}$$

We note that by suitable rescaling of x, t, u and v, it is possible to set $d_1 = c_1 = \tilde{a}_1 = \tilde{b}_1 = 1$ (among other possibilities) in (6), however, we do not do that as it does not result in any significant simplification in the analysis below.

The biological effect of the nonlocal coupling can be attributed to the effect of mobility, e.g., [1]. If species compete for a sparse resource, then due to mobility the inhibiting effect of depletion of this resource should depend not just on the population at a point but on some weighted average of the population [1]. A somewhat different explanation is presented in [7] where it is argued that in population models the spatial point should refer to an average location so that the consumption of resources should be considered not at a point but over an interval encompassing any given spatial location. In [7] spatial nonlocality is further related to the concept of degeneracy, whereby different elements of a system, in this case population in a neighborhood, serve the same function as population at a point in consuming resources. Nonlocality in time is also possible, due to the finite time for species to move and also due to time lag in the recovery of depleted resources, [2,7], however, here we will follow the assumptions in [1,7] that the temporal response of the population is sufficiently rapid that only spatial nonlocality need be considered.

A variety of different kernel functions have been considered in the literature. The simplest assumption is to consider symmetric, unweighted averages over a specified interval, i.e., a step function kernel ϕ_δ, e.g., [8,4,5,7]. A function with a continuous, rather than abrupt, transition from unity to zero is also possible, but if the transition is sufficiently rapid, the transition region can be neglected. It is also possible to consider other kernel functions allowing for a weighted average in the convolutions. Gaussian based functions are considered in [4,5] and exponentials considered in [1,6] (see below). In this paper we consider the stepfunction kernel as well as other kernels which are qualitatively similar to the cutoff Gaussians considered in [4,5] but are simpler to analyze due to the nature of their Fourier transforms.

In our analysis and computations we consider the problem where u and v are periodic on the interval $-L \le x \le L$. The system (1) reduces to the scalar equation of [4,7] if, for example, $v = 0$ or if the parameters of the u and v equations are equal so that if the initial conditions for u and v are equal, we will have $u = v$.

In view of (3) critical points, i.e., spatially uniform stationary solutions $u_\dagger$, $v_\dagger$, satisfy the algebraic system of equations

$$c_1 u_\dagger = u_\dagger (\tilde{a}_1 u_\dagger + \tilde{b}_1 v_\dagger), \tag{7a}$$

$$c_2 v_\dagger = v_\dagger (\tilde{a}_2 u_\dagger + \tilde{b}_2 v_\dagger). \tag{7b}$$

It is clear from (7) that (1) admits a solution $u_\dagger = v_\dagger = 0$ corresponding to extinction of both species. Furthermore, solutions corresponding to extinction of one of the species exist,

$$u_\dagger = \frac{c_1}{\tilde{a}_1}, \qquad v_\dagger = 0, \qquad u_\dagger = 0, \qquad v_\dagger = \frac{c_2}{\tilde{b}_2}. \tag{8}$$

We will always take $\tilde{a}_1 > 0, \tilde{a}_2 > 0, \tilde{b}_1 > 0, \tilde{b}_2 > 0, c_1 > 0$ and $c_2 > 0$ so that these solutions are physical, i.e., the surviving species has a positive population density. These conditions correspond to the standard properties of the logistic equation, namely linear growth and quadratic decay. We note that in [9]

the scalar model with local coupling but with a spatially varying linear growth rate (c_1 in our notation) was studied. The spatial variation connected regions where $c_1 > 0$ (linear growth) with regions where $c_1 < 0$ (linear decay). Islands of existence and effective extinction were found analytically via a matched asymptotic expansion. Nonlocal coupling, for both the scalar problem and the system, as we show here, gives similar results but without the assumption of variable linear birth rate.

The coexistence solution, where both $u_†$ and $v_†$ are nonzero, satisfies

$$c_1 = \tilde{a}_1 u_† + \tilde{b}_1 v_†,$$
$$c_2 = \tilde{a}_2 u_† + \tilde{b}_2 v_†,$$

so that

$$u_† = \frac{-\tilde{b}_1 c_2 + \tilde{b}_2 c_1}{D}, \tag{9a}$$

$$v_† = \frac{\tilde{a}_1 c_2 - \tilde{a}_2 c_1}{D}, \tag{9b}$$

where

$$D = \tilde{a}_1 \tilde{b}_2 - \tilde{a}_2 \tilde{b}_1. \tag{10}$$

We will always assume that the parameters are such that the co-existence solution is physical, i.e., $u_†$ and $v_†$ in (9) are both positive. Furthermore, we will assume that $(u_†, v_†)$ is stable when the coupling is sufficiently local, i.e., when $\delta \to 0$. It can be easily seen that $D > 0$ is necessary and sufficient for $(u_†, v_†)$ to be stable in the case of only local coupling. Thus, we consider the case where $(u_†, v_†)$ is destabilized by the nonlocal interactions.

The focus of this paper will be on cellular structures, i.e., islands of nonzero population, when the coexistence solution is unstable. Thus, for the remainder of this paper we will use the notation $(u_†, v_†)$ to denote only the coexistence critical point. In Section 2 we perform a linear stability analysis about the coexistence critical point. We derive general stability criteria in terms of the parameters and the Fourier transform $\hat{\phi}_\delta$ of the kernel function ϕ_δ. We show that instability cannot occur if $\hat{\phi}_\delta > 0$ for all k, a result shown in [5,7] for the scalar problem, e.g., (6a) with $v = 0$. Thus, the existence of wavenumber bands where $\hat{\phi}_\delta < 0$ is necessary for instability. In particular, instability can occur if $\hat{\phi}_\delta$ is oscillatory around zero, which can happen if, e.g., ϕ_δ has a discontinuity. We then consider three specific kernel functions with support in the interval $|x| < \delta$ (for simplicity we now omit the subscript δ),
(i) stepfunctions

$$\phi_{\text{step}}(x) = \frac{1}{2\delta}, \quad |x| < \delta, \qquad \phi_{\text{step}}(x) = 0, \quad |x| > \delta, \tag{11}$$

(ii) parabolic segments,

$$\phi_p(x) = \frac{3}{4\delta^2}(\delta^2 - x^2), \quad |x| < \delta, \qquad \phi_p(x) = 0, \quad |x| > \delta, \tag{12}$$

and (iii) elevated triangles

$$\phi_{\text{et}}(x) = \frac{\alpha\delta - |x|}{(2\alpha - 1)\delta^2}, \quad |x| < \delta, \qquad \phi_{\text{et}}(x) = 0, \quad |x| > \delta, \tag{13}$$

where $\alpha > 1$ is a free parameter, and show pattern formation when the coexistence critical point is unstable, i.e., for sufficiently large δ.

In Section 3 we consider ϕ_{step}. We show via numerical computations that when $(u_†, v_†)$ is unstable, the solution with initial conditions consisting of a perturbation of $(u_†, v_†)$ evolves to a series of cells, or islands, separated by deadzones where the populations are essentially extinct. All islands are identical, for fixed parameters in (1) the size and spacing of the islands depends only on δ and

the initial conditions. Multiple solutions can occur for different initial conditions. Since all islands are identical, the multiple solutions are characterized by the amplitudes of the islands and their extent, i.e., the period of an individual island/deadzone combination. Despite the intrinsic nonlinearity of these patterns, we are able to obtain a complete and highly accurate approximation using only the parameters of the system and the number of islands within the computational domain (i.e., the period of the island/deadzone structure). In particular, we show that the structure of the islands can be approximated by cosine functions. We then obtain a relationship for the total population within each island that depends only on parameters of the model. Finally we show that the amplitude and extent of each island can be predicted analytically from parameters of the system and the period of the island/deadzone structure.

In Section 4 we consider ϕ_p. We show that for some parameter sets ϕ_p gives significantly more complex patterns than ϕ_{step}, including patterns involving an amplitude modulation of the islands and semi-extinction, i.e., extinction of one of the species. In Section 5 we consider ϕ_{et} and show that this choice of kernel function can lead to tip-splitting within the islands. Finally, in Section 6 we summarize our results.

2. Stability analysis

In this section we determine neutral stability curves and regions in wavenumber space where the critical point $(u_†, v_†)$ is unstable as a function of the Fourier transform $\hat{\phi}$ of the kernel function. We note that it was shown in [1] that for the kernel function

$$\phi(x) = \frac{c}{2} \exp(-c|x|), \tag{14}$$

instabilities can occur for certain parameter regimes, although these regimes and the resulting unstable wavenumber bands were not determined.

We linearize (1) about the coexistence solution $(u_†, v_†)$. Perturbations $\tilde{u}, \tilde{v}$ satisfy the linear integro-differential system

$$\tilde{u}_t = d_1 \tilde{u}_{xx} + (c_1 - \tilde{a}_1 u_† - \tilde{b}_1 v_†)\tilde{u} - u_†(\tilde{a}_1 \phi * \tilde{u} + \tilde{b}_1 \phi * \tilde{v}), \tag{15a}$$

$$\tilde{v}_t = d_2 \tilde{v}_{xx} + (c_2 - \tilde{a}_2 u_† - \tilde{b}_2 v_†)\tilde{v} - v_†(\tilde{a}_2 \phi * \tilde{u} + \tilde{b}_2 \phi * \tilde{v}). \tag{15b}$$

We then Fourier transform in x to obtain (written in matrix/vector form)

$$\frac{d}{dt}\begin{bmatrix}\hat{u}\\\hat{v}\end{bmatrix} = M\begin{bmatrix}\hat{u}\\\hat{v}\end{bmatrix}, \tag{16}$$

$$M = \begin{bmatrix} -\tilde{a}_1 u_† \hat{\phi}(k) - k^2 d_1 & -\tilde{b}_1 u_† \hat{\phi}(k) \\ -\tilde{a}_2 v_† \hat{\phi}(k) & -\tilde{b}_2 v_† \hat{\phi}(k) - k^2 d_2 \end{bmatrix},$$

where k is the Fourier mode number and $\hat{u}$, $\hat{v}$ and $\hat{\phi}$ denote the Fourier transforms of $\tilde{u}$, $\tilde{v}$ and ϕ, respectively. Since we only consider even kernel functions, $\hat{\phi}(k)$ will be real for all k. Furthermore, $\hat{\phi}(0) = 1$ from (3) and for the kernel functions that we consider $\hat{\phi}$ is a function only of $\beta = k\delta$, which we also denote by $\hat{\phi}$. Thus, $M = M(\beta)$ and linear stability requires that the eigenvalues of M be either in the left half plane or on the imaginary axis, conditions equivalent to trace$(M) \le 0$ and det$(M) \ge 0$, i.e.,

$$-(d_1 + d_2)\frac{\beta^2}{\delta^2} - (\tilde{a}_1 u_† + \tilde{b}_2 v_†)\hat{\phi} \le 0, \tag{17a}$$

$$d_1 d_2 \frac{\beta^4}{\delta^4} + (d_2 \tilde{a}_1 u_† + d_1 \tilde{b}_2 v_†)\hat{\phi}\frac{\beta^2}{\delta^2} + u_† v_† D\hat{\phi}^2 \ge 0. \tag{17b}$$

If $\hat{\phi}(\beta) \ge 0$ for all β, then $(u_†, v_†)$ will be stable for all Fourier modes k, a result also obtained for the scalar problem, e.g., [4,5,7].

In particular, there will be no instability if the kernel function is a Gaussian. If $\hat{\phi} < 0$ over some wavenumber interval then regions of instability can occur for certain parameter values and for sufficiently large δ, again consistent with results for the scalar equation. This can happen if, for example, the transform oscillates about zero as it would if the kernel had a discontinuity. Indeed, in [5] it is shown that Gaussian kernel functions with a cutoff can lead to instability for the scalar problem. Since the Fourier transform is a continuous functional of ϕ, oscillatory transforms can occur for appropriately smoothed stepfunction-like kernels. In [4] a family of smooth approximations to both stepfunctions and Gaussians was shown to give rise to instabilities for the scalar problem. The C^0 function (14) (albeit with a discontinuity in the derivative) was considered in [1] where it was shown to lead to instabilities. We show below that a C^0 parabolic kernel function (continuous but with a discontinuity in the derivative) can also allow for instabilities. For (17b) to hold δ must satisfy

$$\frac{1}{\delta^2} \geq -\frac{\hat{\phi}(\beta)}{\beta^2} P \equiv S(\beta), \tag{18}$$

for all β, where

$$P = \frac{1}{2d_1 d_2}\left(d_2 \tilde{a}_1 u_\dagger + d_1 \tilde{b}_2 v_\dagger \right. \\ \left. + \sqrt{(d_2 \tilde{a}_1 u_\dagger - d_1 \tilde{b}_2 v_\dagger)^2 + 4 d_1 d_2 \tilde{a}_2 \tilde{b}_1 u_\dagger v_\dagger} \right).$$

If $\hat{\phi}$ is oscillatory then (18) will fail when δ is sufficiently large, specifically for

$$\frac{1}{\delta^2} < S(\beta_1) \tag{19}$$

where β_1 is the value of β such that $\hat{\phi}(\beta)/\beta^2$ takes its (necessarily negative) global minimum (so that $S(\beta)$ takes a global maximum).

In fact, equality in (19) defines the stability boundary. In order to see this, note that for δ sufficiently small, both conditions (17a) and (17b) hold. As δ increases if (17a) fails then (17b) must have already failed. That is, if there is equality in (17a),

$$-(d_1 + d_2)\frac{\beta^2}{\delta^2} - (\tilde{a}_1 u_\dagger + \tilde{b}_2 v_\dagger)\hat{\phi} = 0, \tag{20}$$

then necessarily

$$d_1 d_2 \frac{\beta^4}{\delta^4} + (d_2 \tilde{a}_1 u_\dagger + d_1 \tilde{b}_2 v_\dagger)\hat{\phi}\frac{\beta^2}{\delta^2} + u_\dagger v_\dagger D\hat{\phi}^2 < 0.$$

Indeed, we have

$$0 < D = \tilde{a}_1 \tilde{b}_2 - \tilde{a}_2 \tilde{b}_1 = \tilde{a}_1 \tilde{b}_2\left(1 - \frac{\tilde{a}_2 \tilde{b}_1}{\tilde{a}_1 \tilde{b}_2}\right) < \tilde{a}_1 \tilde{b}_2,$$

so that it is sufficient to show

$$d_1 d_2 \frac{\beta^4}{\delta^4} + (d_2 \tilde{a}_1 u_\dagger + d_1 \tilde{b}_2 v_\dagger)\hat{\phi}\frac{\beta^2}{\delta^2} + \tilde{a}_1 \tilde{b}_2 u_\dagger v_\dagger \hat{\phi}^2 < 0. \tag{21}$$

Let $\tilde{x} = \delta^2 \hat{\phi}/\beta^2$ and set $\tilde{A} = \tilde{a}_1 u_\dagger$ and $\tilde{B} = \tilde{b}_2 v_\dagger$. Then

$$-(d_1 + d_2) - (\tilde{A} + \tilde{B})\tilde{x} = 0, \tag{22}$$

and we will show

$$d_1 d_2 + (d_2 \tilde{A} + d_1 \tilde{B})\tilde{x} + \tilde{A}\tilde{B}\tilde{x}^2 < 0. \tag{23}$$

Solving (22) for $\tilde{x}$ we find $\tilde{x} = -(d_1 + d_2)/(\tilde{A} + \tilde{B})$. Plugging this into (23) we obtain

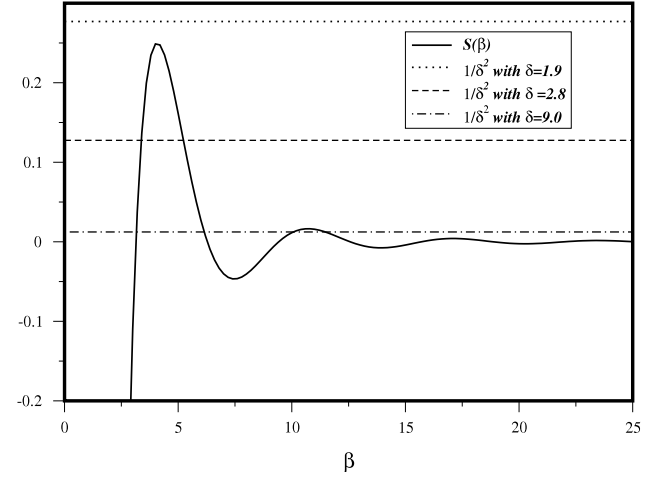$$-\left(\frac{d_1\tilde{B} - d_2\tilde{A}}{\tilde{A} + \tilde{B}}\right)^2 < 0. \tag{24}$$

Fig. 1a. $S(\beta)$ and $1/\delta^2$ for various δ. Parameters given in (25). If $\delta = 1.9$ coexistence critical point $(u_\dagger, v_\dagger)$ is stable. If $\delta = 2.8$ coexistence critical point $(u_\dagger, v_\dagger)$ is unstable, first band. If $\delta = 9.0$ coexistence critical point $(u_\dagger, v_\dagger)$ is unstable, first and second band.

Thus, Eq. (19) establishes the stability boundary and instability arises via a real eigenvalue of M crossing from negative to positive, rather than via a pulsating instability. This result is consistent with our numerical results which show no indication of oscillatory behavior. Our computations for δ near the transition point show that the transition is supercritical. Near the stability boundary only small amplitude, sinusoidal states are found. Furthermore, there is no evidence of bistability of the cellular states with the critical point when δ is below the stability limit. When we follow a cellular branch by decreasing δ below the stability boundary, the only steady state solution that we find is the critical point. When $1/\delta^2 < S(\beta)$ there will be Fourier bands where the matrix $M(\beta)$ has eigenvalues in the right half plane and the coexistence critical point $(u_\dagger, v_\dagger)$ is unstable. These unstable regions are best visualized in Figs. 1a and 1b where we plot $S(\beta)$ against β for the stepfunction and parabolic kernel functions, respectively. For any δ, instabilities correspond to Fourier bands where $S(\beta)$ lies above the horizontal line of height $1/\delta^2$. There may be multiple bands where this occurs, due to the oscillations of $\hat{\phi}$. In the next section we will show that the wavenumbers in the first band accurately predict the size of each island/deadzone region (equivalently the number of islands within a computational domain of size $2L$), even though the island formation that we describe is an intrinsically nonlinear phenomenon, we are operating very far from the stability boundary and the computed patterns are very far from the sinusoidal patterns predicted from the linear stability analysis. Thus, while the linear stability analysis does not predict the structure of the patterns (except near the onset of instability) the unstable wavenumbers are inherited by the nonlinear pattern even far from onset. Such a result is not entirely unexpected, however, in view of the highly nonlinear nature of the patterns it illustrates the power of the linear stability analysis. Generally, we do not find island structures corresponding to bands higher than 1 except in isolated instances.

3. Stepfunction kernel

In this section we describe solution behavior for the stepfunction kernel ϕ_{step} (see (11)). Since this is the only kernel function used in this section, we use the notation ϕ rather than ϕ_{step}. We consider the following parameter set:

$$d_1 = d_2 = 2, \qquad c_1 = 49, \qquad c_2 = 9,$$
$$\tilde{a}_1 = 250, \qquad \tilde{a}_2 = 40, \qquad \tilde{b}_1 = 100, \qquad \tilde{b}_2 = 30, \tag{25}$$
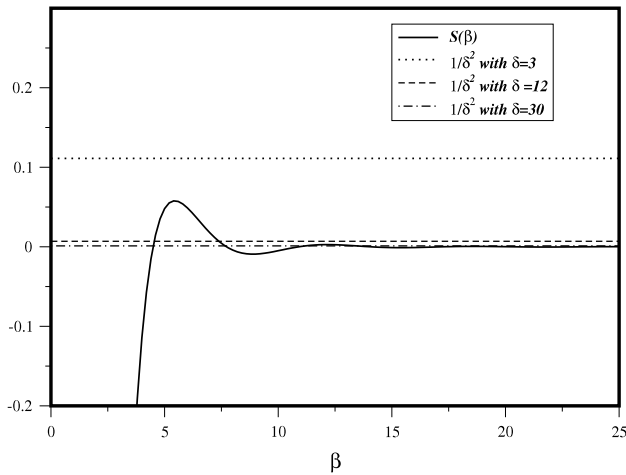
Fig. 1b. $S(\beta)$ and $1/\delta^2$ for various δ. Parameters: $d_1 = 1$, $d_2 = 2$, $c_1 = 49.9$, $c_2 = 9.99$, $\tilde{a}_1 = 49$, $\tilde{a}_2 = 10$, $\tilde{b}_1 = 0.1$, $\tilde{b}_2 = 0.03$. If $\delta = 3$ coexistence critical point $(u_\dagger, v_\dagger)$ is stable. If $\delta = 12$ coexistence critical point $(u_\dagger, v_\dagger)$ is unstable, first band. If $\delta = 30$ coexistence critical point $(u_\dagger, v_\dagger)$ is unstable, first and second band.

with periodicity assumed on the interval $-L \leq x \leq L$ and $L = 1000$. We consider a stepfunction kernel function of extent δ (see (11)) which is the only parameter that we vary. For these parameters, the coexistence critical point is $(u_\dagger, v_\dagger) = (0.1629, 0.0829)$ which is stable for $\delta < 1.8538$ (all numbers rounded to 4 decimal places).

We solve the problem using a Fourier method. The unknowns are updated in Fourier space where the spatial derivatives and convolutions are computed. Nonlinear terms are computed in physical space and then transformed to Fourier space for the solution update. We assume symmetry about $x = 0$. We have tested this assumption and found that we were unable to find different solutions (except for a translation in x) with the symmetry assumption relaxed. Solutions are obtained with various initial conditions, including both perturbations of $(u_\dagger, v_\dagger)$ (both random and deterministic) and continuation in δ. We integrate in time until steady state conditions are obtained. We have only found stationary solutions for the conditions described here.

In order to set the frame of reference, we first illustrate a sample solution. In Fig. 2a we plot a steady state solution obtained for $\delta = 175$. The solution is characterized by eight identical islands of nonzero population separated by what can be thought of as deadzones where the populations are essentially zero. This solution is characteristic of all solutions we have found for stepfunction kernel functions. As δ is varied, the only difference is in the number of islands in the computational domain, the amplitude and the extent of each island. The solution shown in Fig. 2a has 8 islands. For this value of δ we have also found solutions with 6 and 10 islands for different initial conditions. In order to clarify the structure of the island, we plot in Fig. 2b the solution over just one island.

Since these solutions are characteristic of all stationary solutions we have found, we list properties of these island solutions.

1. The islands are symmetric about their midpoint. (We note that they have the structure of a half cosine curve. This will be discussed below.)
2. The extent of the islands is slightly different for the two species. For these parameters the tail of the island includes a small region where species v survives while species u is essentially extinct.
3. The islands are surrounded by deadzones where the populations are vanishingly small. For example, in the deadzone, say at $x = 70$ in Fig. 2a, both u and v are of the order of 10^{-12}. Thus, within each deadzone both species are essentially extinct.
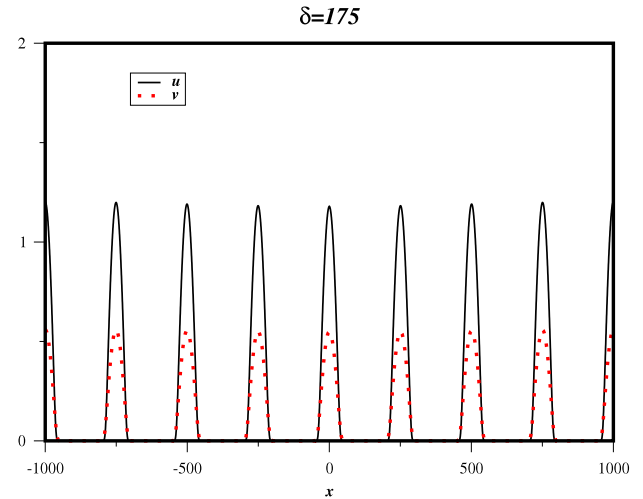

Fig. 2a. Eight island solution for $\delta = 175$. Parameters given in text.
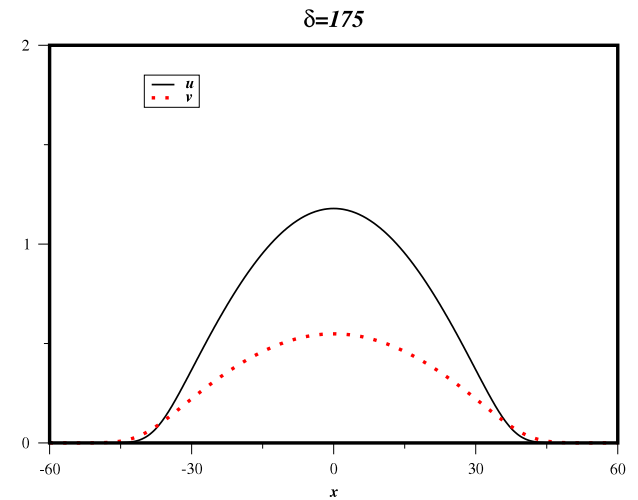

Fig. 2b. Eight island solution for $\delta = 175$. Parameters given in text. Only one island is shown.

This behavior is somewhat surprising in that it is well known that the extinction solution for the logistic equation is unstable. Since each deadzone is of finite extent, infinitely long wavelength disturbances (mode number $k \to 0$) are not possible. Large mode number disturbances can be stabilized by diffusion, however, diffusion is not efficient as k decreases, and such intermediate-scale perturbations can occur when the deadzone is of large extent, such as in Fig. 2a. In this case, we believe that the nonlocal interaction via the convolution integrals in (1) serves to transmit local disturbances away from the deadzone, thus making deadzones of significant extent possible. The size of each deadzone decreases as δ decreases, i.e., as the extent of nonlocality decreases, consistent with this hypothesis. Thus, as δ decreases, effective extinction is confined to smaller and smaller zones.

4. The period of the island/deadzone pattern correlates closely with the unstable wavenumber bands predicted from the linear stability analysis, even though we consider values of δ far from the stability boundary and the resulting patterns are highly nonlinear and very different from the small amplitude sinusoidal type patterns considered in the stability analysis.

We next discuss point 4. As shown above (see especially Fig. 1a), instability occurs when the horizontal line $y = 1/\delta^2$ is below segments of the curve $S(\beta)$. Any interval where this occurs represents an unstable wavenumber band. The wavenumbers within

Table 1
Predicted and computed number of islands.

δ	I range	I for max of band 1	Computed I
5	204–377	260	276
10	101–196	130	152
20	51–99	65	64, 68, 70–72, 76, 80
30	34–66	43	52
50	21–39	26	25, 30
75	14–26	17	18
100	11–19	13	12, 13
125	9–15	10	9, 12
150	7–13	9	8, 9
175	6–11	7	6, 8, 10
200	6–9	7	6–8
250	5–7	5	6
300	4–6	4	4
350	3–5	4	4
400	3–4	3	4

Fig. 3. Transition behavior for the function $G(x)$.

this band provide a mechanism to predict the period of the island/deadzone pair. This prediction can in turn be used to predict the number of islands within a given computational domain. For the parameters in (25) this prediction appears to accurately represent the computed solutions, even though the island/deadzone combinations that we compute clearly represent a highly nonlinear phenomenon (these solutions cannot in any way be considered a small perturbation of the unstable equilibrium point $(u_†, v_†)$, and the solution is far from sinusoidal as would be expected from the linear stability analysis). For the parameters in (25) (the same parameters as used in Fig. 1a) we correlate the predicted range of the number of islands with solutions found numerically in Table 1 (for simplicity we let I denote the number of islands in the computational domain $-L \leq x \leq L$, where $L = 1000$, that we use). We only tabulate data for crossings of the first band, as we have only been able to find one stable island/deadzone solution corresponding to a higher order band.

The data in Table 1 shows a close correlation between the unstable mode numbers and the computed number of islands that we find. The correlation degrades as δ decreases, perhaps due to the fact that there is a wider range of values of I possible. We emphasize that we expect there to be more stable solutions than those indicated in Table 1 as we have tested only a limited number of initial conditions; however, even within this limitation there appears to be a significant multiplicity of stable island/deadzone patterns. Finally, for sufficiently small values of δ, the equilibrium solution $(u_†, v_†)$ is stable. Specifically, for $\delta = 1.8$ we were unable to find any stable solution other than $(u_†, v_†)$ consistent with the linear stability results illustrated in Fig. 1a.

3.1. Analysis of island structure

In this subsection we present an analysis which allows for a description of the structure of individual islands for the case that the global coupling is based on the stepfunction kernel (11).

In order to describe our methodologies, we consider the solution shown Fig. 2a. There are eight islands, each symmetric and each centered at the point

$$x_i = 250i, \quad i = 0, \pm 1, \pm 2, \pm 3, \pm 4.$$

(The islands corresponding to $i = \pm 4$ are each only half contained within the domain $-L \leq x \leq L$ with $L = 1000$.) Since the solution is steady, u and v satisfy

$$d_1 u_{xx} + F(x)u = 0, \tag{26a}$$
$$d_2 v_{xx} + G(x)v = 0, \tag{26b}$$

where

$$F(x) = c_1 - \tilde{a}_1 \phi * u - \tilde{b}_1 \phi * v, \tag{27}$$
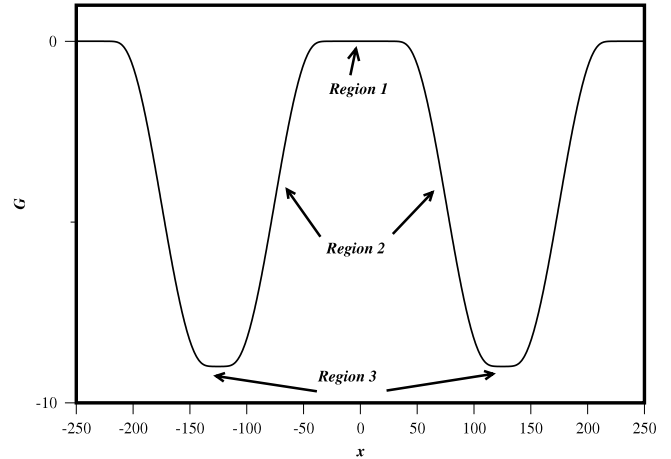$$G(x) = c_2 - \tilde{a}_2 \phi * u - \tilde{b}_2 \phi * v,$$

and we have explicitly indicated the dependence of F and G on x through u and v.

In Fig. 3 we plot G for a region encompassing the island centered at $x = 0$, the two adjacent deadzones and parts of the adjacent islands. The analogous data for u is similar, the data is presented for just one species for simplicity. The function $G(x)$ exhibits three different behaviors over three different regions in x. Region 1 corresponds to the bulk of the island and in this region G is, to a very close approximation, a small positive constant. Region 3 corresponds to the center of the deadzone and in this region G is roughly a large negative constant. (We note that while in Region 1 G and F are constant to at least nine significant figures, in Region 3 G and F are constant to only four significant figures.) Region 2 is a transition region connecting these two regions.

The behavior of G in these regions can be understood from the convolution integrals (2). Since $\delta = 175$, the convolution integrals in Region 1 encompass the entire island centered at $x = 0$ and some fraction of the adjacent deadzones where u and v are zero to within numerical precision. As a result, the convolution integrals that enter into G (and F) are essentially independent of x over most of the island structure. They are simply the means of u and v over the island. (This, of course, would not be the case for convolution kernels other than (11).) Only for values of x near the tails of the island will the convolution integrals incorporate some nonzero values from the adjacent islands. Since the nonlocal coupling enters into the equations with a negative sign, these adjacent islands cause G (and F) to decrease. As x moves further into Region 2, the convolution integrals pick up more of the adjacent islands and still incorporate all of the island centered at $x = 0$ thus, leading to a relatively rapid decrease in G (and F). As x approaches the center of the deadzone (Region 3) the convolution integrals encompass two adjacent islands so that there is no significant x dependence and G and F are essentially large negative constants. In fact, it is these nonlocal terms which stabilize extinction within the deadzone, as extinction is unstable for the logistic model by itself. From (26) we see that u and v satisfy constant coefficient equations in Regions 1 and 3, with sinusoidal behavior expected in Region 1 and exponential behavior expected in Region 3, and an Airy Function type transition region connecting the two constant coefficient regions.

We note that our computations show that u and v are zero to within any reasonable numerical precision in the deadzone. Thus, we cannot determine whether the solution in this region is exponentially small or just zero. Since at steady state u and v satisfy the second order linear differential equation (26), we expect that u and v are nonzero in the deadzones, but at a level so small that it cannot be resolved numerically.

In Region 1 we can rewrite (26) as

$$u_{xx} + \Omega_u^2 u = 0, \tag{28a}$$

$$v_{xx} + \Omega_v^2 v = 0, \tag{28b}$$

where

$$\Omega_u^2 = \frac{c_1 - \tilde{a}_1 \phi * u - \tilde{b}_1 \phi * v}{d_1},$$

$$\Omega_v^2 = \frac{c_2 - \tilde{a}_2 \phi * u - \tilde{b}_2 \phi * v}{d_2}, \tag{29}$$

and Ω_u and Ω_v are independent of x.

In view of (28) u and v can be approximated in Region 1 by

$$u = A_u \cos(x\Omega_u), \qquad v = A_v \cos(x\Omega_v), \tag{30}$$

for $|x\Omega_u| < \frac{\pi}{2}$ and $|x\Omega_v| < \frac{\pi}{2}$, respectively. Eq. (30) will only be inaccurate for values of x near the tails of the islands where u and v are approaching zero and the convolution integrals incorporate a contribution from adjacent islands. Here A_u and A_v are the amplitudes of the islands. Using (30), the convolutions $\phi * u$ and $\phi * v$ are

$$\phi * u = \frac{A_u}{\delta \Omega_u}, \qquad \phi * v = \frac{A_v}{\delta \Omega_v}. \tag{31}$$

Thus, Ω_u^2 and Ω_v^2 in (29) are not determined explicitly, but rather are themselves functions of Ω_u and Ω_v. Using (31) in (29) results in a coupled system of algebraic equations for Ω_u and Ω_v,

$$d_1 \Omega_u^3 = c_1 \Omega_u - \tilde{a}_1 \frac{A_u}{\delta} - \tilde{b}_1 \frac{\Omega_u A_v}{\delta \Omega_v}, \tag{32a}$$

$$d_2 \Omega_v^3 = c_2 \Omega_v - \tilde{a}_2 \frac{\Omega_v A_u}{\delta \Omega_u} - \tilde{b}_2 \frac{A_v}{\delta}. \tag{32b}$$

Eqs. (32) can be readily solved as an algebraic system of equations (it can also be reduced to a ninth degree polynomial for either Ω_u or Ω_v). It is more instructive to reformulate (32) for the ratios

$$R_u = \frac{A_u}{\Omega_u}, \qquad R_v = \frac{A_v}{\Omega_v}. \tag{33}$$

We note that $2R_u$ and $2R_v$ are simply the total population of species u and v, respectively, within the island, subject to the cosine approximation in (30). We have

$$R_u = \frac{\delta}{D} \left[\tilde{b}_2 c_1 - \tilde{b}_1 c_2 + \tilde{b}_2 d_1 \Omega_u^2 - \tilde{b}_1 d_2 \Omega_v^2 \right], \tag{34a}$$

$$R_v = \frac{\delta}{D} \left[\tilde{a}_1 c_2 - \tilde{a}_2 c_1 + \tilde{a}_2 d_1 \Omega_u^2 - \tilde{a}_1 d_2 \Omega_v^2 \right], \tag{34b}$$

where D is given in (10). The extent of the islands in the cosine approximation (30) are π/Ω_u and π/Ω_v, for u and v respectively. Our assumption leading to (30) (supported by numerical computations) is that the islands are of extent $O(\delta)$. It follows that Ω_u^2 and Ω_v^2 are small compared to the leading order terms in (34a) and (34b). Neglecting these terms gives an estimate for the population within each island solely in terms of δ and the kinetic parameters of the model,

$$R_u/\delta \simeq \frac{\tilde{b}_2 c_1 - \tilde{b}_1 c_2}{D}, \tag{35a}$$

$$R_v/\delta \simeq \frac{\tilde{a}_1 c_2 - \tilde{a}_2 c_1}{D} \tag{35b}$$

The estimates (35) agree closely with computed values as can be seen in Table 2 for a representative sampling of our computed solutions (recall that I is the computed number of islands in the

Table 2
Computed and predicted values of R_u/δ and R_v/δ.

δ	I	R_u/δ	I_u/δ	(35a)
100	12	0.1629	0.1629	0.1629
175	6	0.1629	0.1628	0.1629
175	8	0.1629	0.1628	0.1629
175	10	0.1632	0.1633	0.1629
200	6	0.1629	0.1628	0.1629
300	4	0.1629	0.1628	0.1629
400	4	0.1629	0.1627	0.1629

δ	I	R_v/δ	I_v/δ	(35b)
100	12	0.08264	0.08264	0.08286
175	6	0.08282	0.08278	0.08286
175	8	0.08269	0.08263	0.08286
175	10	0.08162	0.08150	0.08286
200	6	0.08280	0.08276	0.08286
300	4	0.08283	0.08279	0.08286
400	4	0.08276	0.08268	0.08286

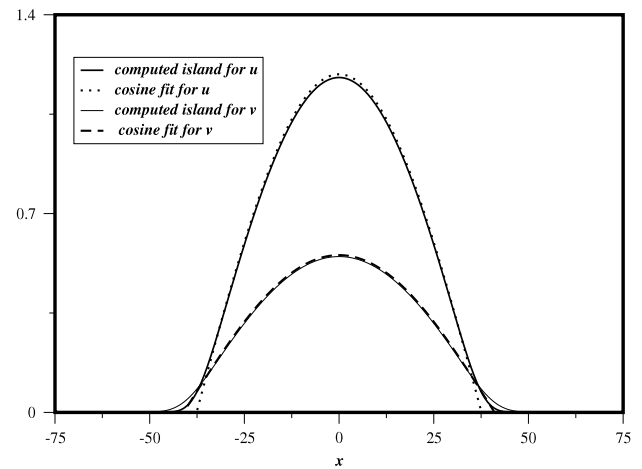**Fig. 4.** Comparison of island structure with cosine fit obtained from (32).

computational domain). For entry in the table the values of R_u/δ and R_v/δ are computed from the cosine approximation with the amplitudes A_u and A_v taken from the computed solutions, while Ω_u and Ω_v were obtained from a numerical solution of the system (32) and choosing the root pair where Ω_u and Ω_v were both positive and where their sum was minimized (since we expect them to be small). (We note that since (32) can be reduced to a ninth degree polynomial there are at most nine real root pairs.) The quantities I_u/δ and I_v/δ in the table represent the integrals of the computed numerical solution over half of the island normalized by δ.

We illustrate the accuracy of the cosine fit in Fig. 4 where we plot the computed cosine fit against the numerical solution for the 8-island case with $\delta = 175$. We note that the results shown in Fig. 4 are typical of results that we have obtained for many other parameter sets as well. These results demonstrate that the methodology described above can successfully reproduce the computed island structure. However, the methodology, while providing for scaling laws for the total population within each island, has several significant limitations when employed to reconstruct specific solutions— (i) it is restricted to a stepfunction kernel function, (ii) it requires knowledge of the numerically computed amplitudes of the islands, (iii) the cosine reconstruction does not capture the transitions to the adjacent deadzones, and (iv) extraneous root pairs of the system (32) have to be excluded. Point (iv) can be addressed by assuming small Ω_u and Ω_v and using the procedure to choose the proper root pair described above. In terms of point (i) above, at this time we are only able to obtain a complete analysis for the stepfunction kernel function. As will be seen below, other kernel functions generally give a more complicated structure for the islands, e.g.,

tip-splitting or an amplitude modulation. A matched expansion connecting the cosine approximation to an exponential decay via an Airy function transition region (analogous to the expansion in [9]) could, in principle, address point (iii) above; however, for the parameters that we consider we have not been able to obtain satisfactory accuracy from such an expansion. It is possible to address point (ii) above, i.e., determine properties of the islands without using computed information, albeit with some loss of accuracy. We consider this directly below.

In view of (34) estimates for the amplitudes A_u and A_v can be obtained once estimates for Ω_u and Ω_v have been obtained. In order to obtain such estimates, we refer to Fig. 3 and observe that the end of the regions where the cosine approximation is valid (regions where F and G are essentially positive constants) is close to the points where F and G are zero. There is certainly a transition region, however, the extent of the transition region is small compared to the extent of the island as can be seen from the figure (this is also the case for other island/deadzone solutions that we have computed). Considering an island centered at $x = 0$ (see Fig. 4), we employ the cosine approximation (30) in (27) and determine Ω_u and Ω_v from the condition

$$F(x_u) = 0, \qquad G(x_v) = 0 \tag{36}$$

where

$$x_u = \frac{\pi}{2\Omega_u}, \qquad x_v = \frac{\pi}{2\Omega_v}.$$

We therefore have

$$c_1 = \tilde{a}_1 \phi * u(x_u) + \tilde{b}_1 \phi * v(x_u), \tag{37a}$$

$$c_2 = \tilde{a}_2 \phi * u(x_v) + \tilde{b}_2 \phi * v(x_v), \tag{37b}$$

where we use the fact that the two convolutions are the only x-dependent terms in F and G.

We define ℓ as the center of the island immediately to the right of the island centered at $x = 0$, so that ℓ is simply the period of the island/deadzone structure, $\ell = 2L/I$. In this island the cosine approximation is

$$u = A_u \cos(\Omega_u(x - \ell)), \qquad v = A_v \cos(\Omega_v(x - \ell)). \tag{38}$$

Since we can take u and v to be zero in the deadzone separating the two islands, we then have

$$\phi * u(x_u) = \frac{1}{2\delta} \int_{x_u - \delta}^{x_u} A_u \cos(\Omega_u x) dx$$
$$+ \frac{1}{2\delta} \int_{\ell - x_u}^{x_u + \delta} A_u \cos(\Omega_u(x - \ell)) dx, \tag{39}$$

with similar expressions for $\phi * u(x_v)$, $\phi * v(x_u)$, and $\phi * v(x_v)$.

We assume that the extent of each island is less than δ, which is the case for all of the solutions that we have found. Thus, the first integral in (39) is merely the integral of the upper half of a cosine wave and we have

$$\phi * u(x_u) = \frac{2R_u}{2\delta} + \frac{R_u}{2\delta}(1 + \cos(\Omega_u(\delta - \ell)))$$
$$= \frac{R_u}{2\delta}(3 + \cos(\Omega_u(\delta - \ell))), \tag{40}$$

together with the analogous result for v,

$$\phi * v(x_v) = \frac{R_v}{2\delta}(3 + \cos(\Omega_v(\delta - \ell))), \tag{41}$$

where R_u and R_v are defined in (33). Using similar arguments we have

$$\phi * u(x_v) = \frac{R_u}{2\delta}(3 + \sin(\Omega_u(x_v + \delta - \ell))), \tag{42a}$$

$$\phi * v(x_u) = \frac{R_v}{2\delta}(3 + \sin(\Omega_v(x_u + \delta - \ell))). \tag{42b}$$

We next consider approximations for x_u and x_v. Our computations indicate that the extent of the dead zone is generally close to δ. Assuming that the extent of the dead zone is exactly δ we have

$$x_u = x_v = \frac{\ell - \delta}{2},$$

so that

$$\Omega_u = \Omega_v = \tilde{\Omega}_u = \tilde{\Omega}_v = \frac{\pi}{\ell - \delta}, \tag{43}$$

where we use $\tilde{\Omega}_u$ and $\tilde{\Omega}_v$ to denote the approximate value of Ω_u and Ω_v, respectively.

While (43) is close to results from our computations, it does not allow for the island extent to differ for the two species. In addition, for all of our computations the island extent is greater than that obtained from (43). We therefore assume that

$$\Omega_u(\ell - \delta) = \pi + \epsilon_1, \tag{44a}$$

$$\Omega_v(\ell - \delta) = \pi + \epsilon_2, \tag{44b}$$

where ϵ_1 and ϵ_2 are assumed small and we look for solutions where $\epsilon_1 < 0$ and $\epsilon_2 < 0$ consistent with our numerical results.

Using (44) in (41) and (42) and keeping only linear and quadratic terms in ϵ_1 and ϵ_2 yields

$$\phi * u(x_u) = \frac{R_u}{\delta} + \frac{R_u \epsilon_1^2}{4\delta}, \tag{45a}$$

$$\phi * v(x_v) = \frac{R_v}{\delta} + \frac{R_v \epsilon_2^2}{4\delta}, \tag{45b}$$

$$\phi * u(x_v) = R_u \left[\frac{1}{\delta} + \frac{\epsilon_1^2}{16\delta} + \frac{\epsilon_1 \epsilon_2}{8\delta} + \frac{\epsilon_2^2}{16\delta} \right], \tag{45c}$$

$$\phi * v(x_u) = R_v \left[\frac{1}{\delta} + \frac{\epsilon_1^2}{16\delta} + \frac{\epsilon_1 \epsilon_2}{8\delta} + \frac{\epsilon_2^2}{16\delta} \right]. \tag{45d}$$

Using (45) together with (34) expanded to retain only linear and quadratic terms in ϵ_1 and ϵ_2 in (37) results in a system of two quadratic equations in ϵ_1 and ϵ_2. The coefficients involve only the kinetic parameters of the model, δ and ℓ. Since ℓ is simply the period of each island/deadzone structure, it can be obtained simply from the length of the domain L together with the number of islands within each domain. The specific equations, obtained via Mathematica, are given in the Appendix. For all values of δ that we have considered all of the four root pairs of this system are real and there is only one root pair where ϵ_1 and ϵ_2 are both negative. We use this root pair in (44), since, as indicated above, we always find that the island extent is greater than that given by (43).

An illustration of the accuracy of this reconstruction is shown in Fig. 5 for the same case as shown in Fig. 4. The accuracy of the amplitude fit is only slightly degraded from that shown in Fig. 4 where computed amplitude information was employed.

Finally, we compare amplitudes calculated analytically and via numerical computations for the same solutions tabulated in Table 2. After obtaining ϵ_1 and ϵ_2 we compute Ω_u and Ω_v from (44), then R_u and R_v from (41) and then use (34) to compute A_u and A_v. The results are tabulated in Table 3.

4. Parabolic kernel function

We next consider results for the parabolic kernel function (12). All computations in this section were done with $\delta = 175$ and $L = 1000$, however, we employed two different basic parameter sets. For the parabolic kernel function, we found that the computed steady state patterns were very sensitive to initial conditions, leading to a very large multiplicity of steady states. This was true
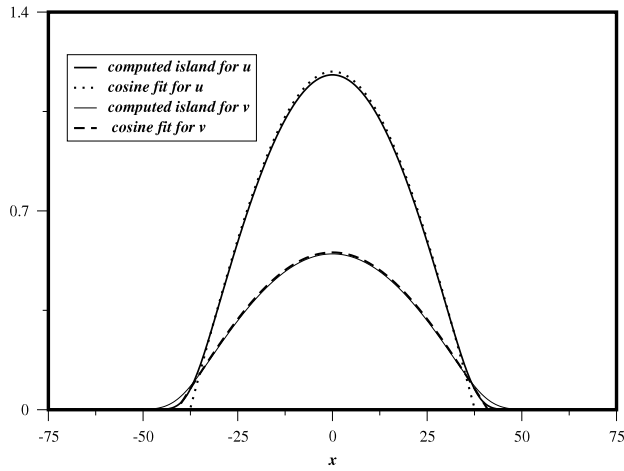
Fig. 5. Comparison of island structure with cosine fit obtained from (45) and the subsequent analysis described in the text.

Table 3
Computed and predicted amplitudes.

δ	I	A_u from analysis	A_u from computations
100	12	0.7678	0.7647
175	6	0.5655	0.5646
175	8	1.1943	1.1899
175	10	3.5916	3.5528
200	6	0.7675	0.7660
300	4	0.7675	0.7664
400	4	2.0470	2.0414

δ	I	A_v from analysis	A_v from computations
100	12	0.3752	0.3819
175	6	0.2832	0.2852
175	8	0.5865	0.5957
175	10	1.6147	1.6983
200	6	0.3831	0.3864
300	4	0.3856	0.3878
400	4	1.0148	1.0266

Fig. 6. Eight array island structure for parabolic kernel function.

Fig. 7. Pattern exhibiting sinusoidal modulation of islands.

both when we used deterministic initial conditions and when we used random initial conditions where different results were found for different seeds. We describe here a sampling of the patterns that we have found.

Employing the parameter set (25), we found patterns consisting of arrays of islands of different amplitudes. One such example is shown in Fig. 6. The solution consists of eight arrays, each composed of three islands. Each array consists of a larger amplitude island surrounded by two smaller amplitude islands. We note that while the amplitude of the islands for species v is smaller than that for species u, the island structure for species v is slightly more extensive than for species u, thus indicating that for these parameters there are solutions such that v can survive in regions where species u cannot. This was also the case for solutions obtained with the stepfunction kernel (see Fig. 2b). It is also the case for other patterns shown in this section.

Using other initial conditions we obtained a pattern that was the reverse of the pattern shown in Fig. 6, eight arrays of three islands each, but now each array consists of two larger and one smaller island. Using still other initial conditions we found patterns consisting of islands with a sinusoidal modulation in their amplitudes. One such pattern is shown in Fig. 7.

For other initial conditions we found an island structure consisting of 32 islands. The pattern looks similar to that obtained with the stepfunction kernel. The number of islands characterizes this solution as corresponding to the third band on the stability diagram (see Fig. 1b). In this case there was very definitely not extinction between the islands, as the solution minima are about 0.0002 and
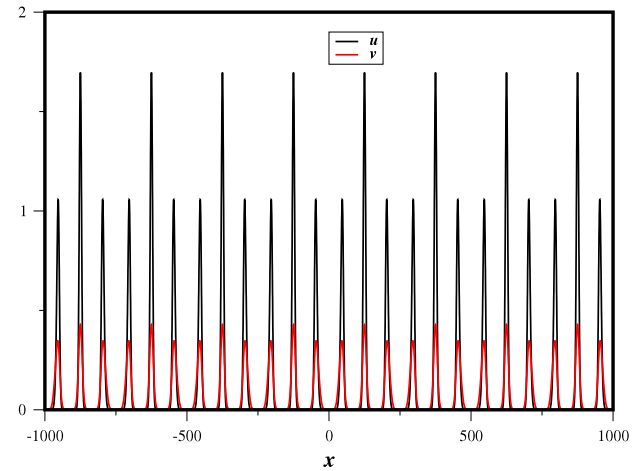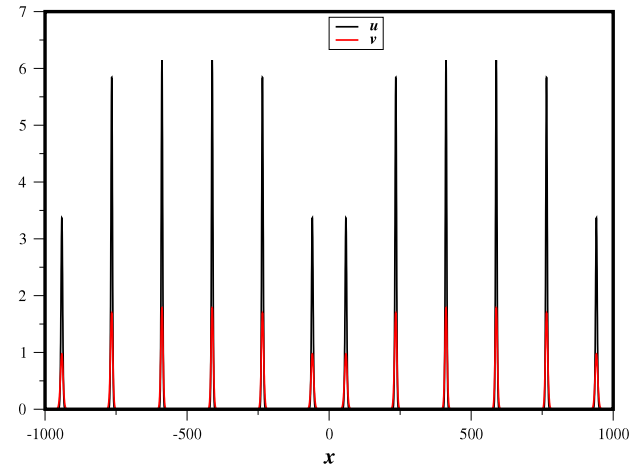
0.01 for u and v, respectively. Thus, for these parameters species v can survive better in the "near"-deadzones, even though the amplitude of the islands for species v is smaller than for species u. Finally, for other initial conditions we were able to find conventional island/deadzone structure similar to that obtained with the stepfunction kernel.

We have found new phenomena using a different set of basic parameters. Specifically, we employed the parameters

$$d_1 = 1, \qquad d_2 = 2, \qquad c_1 = 49.9, \qquad c_2 = 9.99,$$
$$\tilde{a}_1 = 50, \qquad \tilde{a}_2 = 10, \qquad \tilde{b}_1 = 0.1, \qquad \tilde{b}_2 = 0.03.$$

The coexistence critical point is now $(u_\dagger, v_\dagger) = (0.996, 1)$. We found a semi-extinction solution (Fig. 8). There are now 11 islands for u, but v is essentially zero (v is of order 10^{-15}). We note that the semi-extinction critical point for the system of ordinary differential equations (i.e., without diffusion and nonlocal coupling) with these parameters is $u_{\dagger\dagger} = 49.9/50 \simeq 1$, $v_{\dagger\dagger} = 0$ and is unstable. We have also computed this solution with the same initial data for u, but with the initial condition for v set to zero. The result is the same solution for u, but with v identically equal to zero. Thus, this semi-extinction solution is also a solution of the scalar Eq. (1a) with v identically zero. We also note that using the stepfunction kernel with these parameters and initial conditions led to a conventional island/deadzone solution.

We found another semi-extinction solution shown in Fig. 9, using other initial conditions. Here there are eight arrays, each consisting of three islands of variable height (similar to Fig. 6) for u, while v is essentially 0 (again of the order of 10^{-15}).
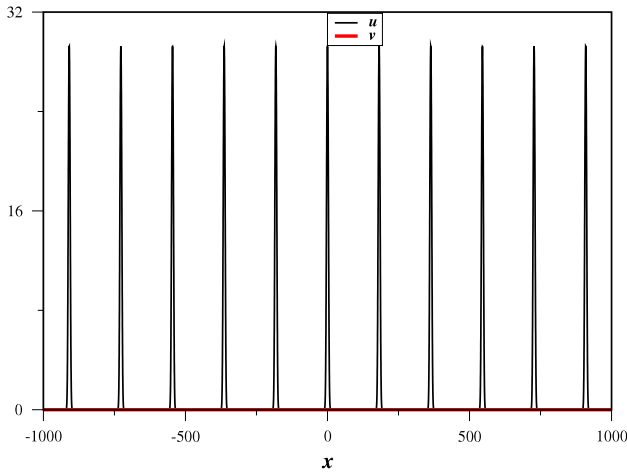
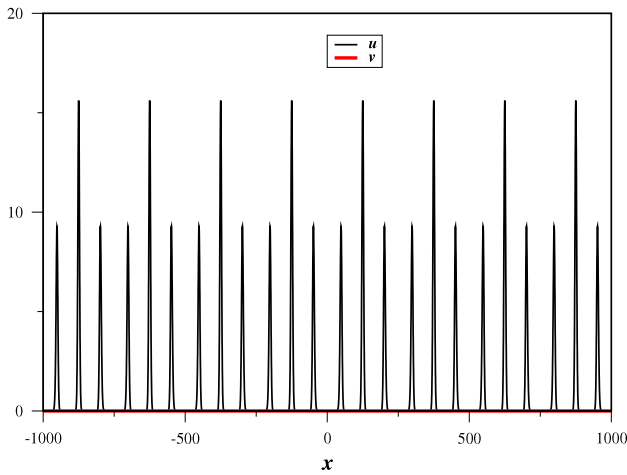**Fig. 8.** Semi-extinction solution for parabolic kernel function.

Fig. 9. Semi-extinction solution consisting of eight arrays.

Fig. 10. Solution exhibiting tip-splitting using ϕ_{et} with $\alpha = 3$. Parameters given in (25).

We have not been able to find a conventional island/deadzone structure for these parameters and the parabolic stepfunction. We did find a 32-island structure, corresponding to a higher order band in the stability diagram. For this solution there are no strict deadzones, the solution is at a low level, but one within what we believe is the accuracy of the computation (the minimum value for v is roughly 0.002 while the minimum for u is roughly 3.7×10^{-5}). As we found for other parameters (see above), v is larger than u in the "near"-deadzones, even though it appears to be the species most prone to extinction for these parameters.

5. Elevated triangle kernel functions and tip-splitting

In this section we show that the use of ϕ_{et} can lead to tip-splitting within the islands. We employ the same parameters as in (25) with $\delta = 175$. A solution exhibiting tip-splitting is shown in Fig. 10. Tip-splitting is very prevalent with the use of ϕ_{et} and this solution is just one of many that we have computed exhibiting such a structure.

6. Conclusion

We have studied a model of competing populations with non-local interactions. The system that we consider is a two-species extension of the Fisher equation with the nonlocality due to convolution integrals against specified kernel functions extending over an interval 2δ. All of our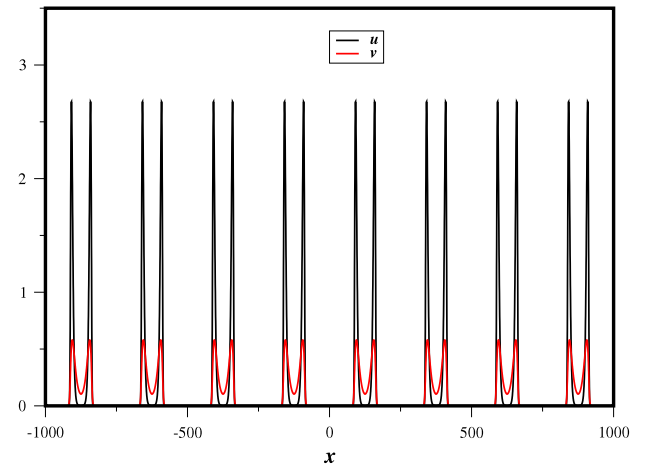 kernel functions are even and of compact support. We consider only the case where the coexistence equilibrium solution, $(u_\dagger, v_\dagger)$, spatially homogeneous and independent of time, is stable for local interactions ($\delta \to 0$) and is destabilized by the nonlocal interactions (i.e., δ sufficiently large). We note that it is not necessary for the kernel function to be of compact support. For example, it could be a Gaussian or some modification of a Gaussian. In this case δ represents a characteristic length scale associated with the kernel function.

A linear stability analysis shows that if the Fourier transform of the convolution kernel function becomes negative there can be bands of wavenumbers where instability occurs and pattern formation is expected. We have found nonlinear patterns by solving the system numerically with initial conditions that are a small perturbation of the unstable equilibrium $(u_\dagger, v_\dagger)$ until steady state solutions are obtained. The resulting patterns are truly nonlinear, being far from a perturbation of $(u_\dagger, v_\dagger)$ although the wavenumbers associated with the unstable band from the linear stability analysis provide an accurate indicator of the spatial period of the patterns. The most prominent pattern we find is that of an island/deadzone structure, where a series of islands of nonzero population is separated by deadzones where the population is essentially zero.

For a stepfunction kernel, all patterns that we have been able to find consist of an array of identical island/deadzones. We have analyzed the structure of the islands and shown that they can be approximated by the positive half of a cosine wave. For fixed parameters a multiplicity of island/deadzone solutions are possible depending on initial conditions. The solutions differ only in the island amplitude and the number of islands within our computational domain (i.e., the period of the island/deadzone pattern). Furthermore, we have developed scaling relations which predict, to a close approximation, the total population of each island in terms of parameters of the model. Finally, we are able to estimate properties of the island, i.e., the amplitude and extent, in terms of parameters of the problem and the period of the island/deadzone pattern. These estimates exhibit close agreement with numerical computations.

For other convolution functions that we have examined, we still find in most instances an island/deadzone structure, but with a modulation in the amplitude of the islands. In some cases this modulation is sinusoidal while in other cases the modulation is manifested in a grouping of the islands into arrays, with each array exhibiting a specified pattern of amplitudes. We also find instances of tip-splitting of the island, so that within each island there is a "near"-deadzone, where the populations are small, but greater than zero. Finally, for some parameters we find semi-extinction patterns, where one of the species is extinct while the

other species exhibits an island/deadzone behavior. As for the stepfunction kernel, for fixed parameters a large multiplicity of different steady state patterns can be obtained depending on initial conditions.

Acknowledgment

Appendix

Using (44) in (41) and expanding up to quadratic terms in ϵ_1 and ϵ_2 yields

$$R_u = \frac{\delta}{D}\left\{\left[\tilde{b}_2 c_1 - \tilde{b}_1 c_2\right]\right.$$
$$\left. - \left[\tilde{b}_2 d_1\left(\frac{\pi + \epsilon_1}{\ell - \delta}\right)^2 - \tilde{b}_1 d_2\left(\frac{\pi + \epsilon_2}{\ell - \delta}\right)^2\right]\right\}, \tag{A.1a}$$

$$R_v = \frac{\delta}{D}\left\{\left[\tilde{a}_1 c_2 - \tilde{a}_2 c_1\right]\right.$$
$$\left. - \left[\tilde{a}_2 d_1\left(\frac{\pi + \epsilon_1}{\ell - \delta}\right)^2 - \tilde{a}_1 d_2\left(\frac{\pi + \epsilon_2}{\ell - \delta}\right)^2\right]\right\}. \tag{A.1b}$$

Using (A.1) together with (44) in (45) and keeping only linear and quadratic terms in ϵ_1 and ϵ_2 results in the coupled system of quadratic equations

$$0 = \frac{d_1 \pi^2}{(\ell - \delta)^2} + \frac{2 d_1 \pi \epsilon_1}{(\ell - \delta)^2} + A_{11}\epsilon_1^2 + A_{12}\epsilon_1\epsilon_2 + A_{22}\epsilon_2^2, \tag{A.2a}$$

$$0 = \frac{d_2 \pi^2}{(\ell - \delta)^2} + \frac{2 d_2 \pi \epsilon_2}{(\ell - \delta)^2} + B_{11}\epsilon_1^2 + B_{12}\epsilon_1\epsilon_2 + B_{22}\epsilon_2^2, \tag{A.2b}$$

where

$$A_{11} = -Z\left[\tilde{a}_2\tilde{b}_1 d_1\left(16 + \pi^2\right) - \tilde{a}_1\tilde{b}_2 d_1\left(16 + 4\pi^2\right)\right.$$
$$+ 3\tilde{a}_1\tilde{b}_1\left((d_2\pi^2 - c_2)(\ell - \delta)^2\right)$$
$$\left. + c_1(\ell - \delta)^2\left(4\tilde{a}_1\tilde{b}_2 - \tilde{a}_2\tilde{b}_1\right)\right],$$

$$A_{12} = -Z\left[\pi^2\left(2\tilde{a}_2\tilde{b}_1 d_1 - 2\tilde{a}_1\tilde{b}_1 d_2\right)\right.$$
$$\left. + (\ell - \delta)^2\left(2\tilde{a}_1\tilde{b}_1 c_2 - 2\tilde{a}_2\tilde{b}_1 c_1\right)\right],$$

$$A_{22} = -Z\left[\pi^2\left(\tilde{a}_2\tilde{b}_1 d_1 - \tilde{a}_1\tilde{b}_1 d_2\right) + (\ell - \delta)^2\left(\tilde{a}_1\tilde{b}_1 c_2 - \tilde{a}_2\tilde{b}_1 c_1\right)\right],$$

$$B_{11} = -Z\left[\pi^2\left(\tilde{a}_2\tilde{b}_1 d_2 - \tilde{a}_2\tilde{b}_2 d_1\right) + (\ell - \delta)^2\left(\tilde{a}_2\tilde{b}_2 c_1 - \tilde{a}_2\tilde{b}_1 c_2\right)\right],$$

$$B_{12} = -Z\left[\pi^2\left(2\tilde{a}_2\tilde{b}_1 d_2 - 2\tilde{a}_2\tilde{b}_2 d_1\right)\right.$$
$$\left. + (\ell - \delta)^2\left(2\tilde{a}_2\tilde{b}_2 c_1 - 2\tilde{a}_2\tilde{b}_1 c_2\right)\right],$$

and

$$B_{22} = -Z\left[\left(\tilde{a}_2\tilde{b}_1 d_2\right)\left(16 + \pi^2\right) - \tilde{a}_1\tilde{b}_2 d_2\left(16 + 4\pi^2\right)\right.$$
$$+ 3\tilde{a}_2\tilde{b}_2\left(d_1\pi^2 - c_1(\ell - \delta)^2\right)$$
$$\left. + c_2(\ell - \delta)^2\left(4\tilde{a}_1\tilde{b}_2 - \tilde{a}_2\tilde{b}_1\right)\right],$$

where

$$Z = \frac{1}{16D(\ell - \delta)^2}.$$

For the parameters used in Fig. 5 the system of quadratics is

$$0 = 0.00007019 + 0.0000446804\epsilon_1 - 0.213983\epsilon_1^2$$
$$- 0.0206616\epsilon_1\epsilon_2 - 0.0103308\epsilon_2^2 = 0, \tag{A.3a}$$

$$0 = 0.000350919 + 0.000223402\epsilon_2 - 0.0407318\epsilon_1^2$$
$$- 0.0814637\epsilon_1\epsilon_2 - 0.102681\epsilon_2^2 = 0, \tag{A.3b}$$

which has the single pair of negative roots $(\epsilon_1, \epsilon_2) = (-0.0115445, -0.0526148)$.

References

[1] N.F. Britton, Aggregation and the competitive exclusion principle, J. Theoret. Biol. 136 (1989) 57–66.
[2] N.F. Britton, Spatial structures and periodic travelling waves in an integro-differential reaction–diffusion population model, SIAM J. Appl. Math. 50 (1990) 1663–1688.
[3] Y.E. Marukva, N.M. Shnerb, Nonlocal competition and logistic growth: patterns, defects and fronts, Phys. Rev. E 73 (2006) 011903.
[4] M.A. Fuentes, M.N. Kuperman, V.M. Kenkre, Nonlocal interaction effects on pattern formation in population dynamics, Phys. Rev. Lett. 91 (#15) (2003) 158104-1–158104-4.
[5] M.A. Fuentes, M.N. Kuperman, V.M. Kenkre, Analytical considerations in the study of spatial patterns arising from nonlocal interaction effects, J. Phys. Chem. B 108 (2004) 10505–10508.
[6] S.A. Gourley, M.A.J. Chaplain, F.A. Davidson, Spatio-temporal pattern formation in a nonlocal reaction–diffusion equation, Dyn. Syst. 16 (2001) 173–192.
[7] S. Genieys, V. Volpert, P. Auger, Pattern and waves for a model in population dynamics with nonlocal consumption of resources, Math. Model. Nat. Phenom. 1 (2006) 63–80.
[8] J. Furter, M. Grinfeld, Local vs. non-local interactions in population dynamics, J. Math. Biol. 27 (1989) 65–80.
[9] N. Kumar, V.M. Kenkre, Effects of gradual spatial variation in resources on population extinction: analytic calculations for abrupt transitions, Physica A 390 (2011) 257–262.